

# Shear strength reduction in triaxial compression of confined granular materials due to vibrations using the discrete element method.

R. B. Andrade<sup>1</sup>, G. Koval<sup>2</sup>, G. H. Siqueira<sup>1</sup>

<sup>1</sup>*Departamento de estruturas e geotecnia, Univerisade Estadual de Campinas  
Rua Saturnino de Brito, 224, Cidade Universitária Zeferino Vaz, Campinas - São Paulo  
rodrigo31ba@gmail.com, siqueira@fec.unicamp.br*

<sup>2</sup>*Laboratoire ICUBE, Equipe GC-E, Institut National des Sciences Appliquées de Strasbourg  
24 bld de la Victoire, 67000 Strasbourg, France  
georg.koval@insa-strasbourg.fr*

**Abstract.** When subjected to external forces, the mechanical behavior of granular materials may range from static to dynamic. Unconfined granular beds, for example, are easily fluidized by vibratory loading. Under confinement, this type of material may also exhibit observable effects due to vibrations regarding their volumetric and strength behaviors. In this paper, the shear strength and dilatancy of dry confined granular materials subjected to vibrations are investigated using discrete element simulations of a triaxial cell. The material is first subjected to isotropic compression. Then, with controlled lateral stresses and imposed vertical motion, shear and compressive stresses are applied to a cubic sample. Next, harmonic vibration of the cell induces vertical and horizontal vibrations in the system while the confinement stress is maintained. The imposed vibration led to shear strength reduction and a decrease in volumetric strain. The effect of the vibration was greater at the beginning of the vibration phase, with a smaller effect as time progressed. The impact of frequency and amplitude on internal friction angle reduction was assessed, showing that these are relevant parameters for the behavior of confined granular materials under vibration.

**Keywords:** granular materials, triaxial shear, fluidization, DEM

## 1 Introduction

The mechanical response of granular materials exhibits a complex range of behaviors under both static and dynamic conditions. Notably, these materials can undergo sudden changes in response, such as fluidization due to fluid flow, cyclic loading, or vibration excitation.

Vibrations may affect the mechanical behavior of granular materials in several ways [1]. In granular beds the effect of vibration may include segregation, convection, and vibro-fluidization [2, 3]. While vibration in granular beds have been more thoroughly studied due to their relevance in industrial applications, the effect of vibrations in other granular materials is less understood. It is known that vibrations of confined granular materials may affect its strength, friction between grains and dilatancy [4, 5], to the point of fluidizing the material [6] even though the effect of amplitude, frequency, and direction of the vibrations on the mechanical properties of confined granular materials is not perfectly understood, and proposals for the description of the phenomena are still being developed [e.g. 7–9].

Understanding the impact of vibrations in confined granular material may be useful for many science and engineering applications. In geophysics, the coupling of frictional sliding and vibrations is relevant for the description of fault dynamics [10, 11]. In astrophysics, the response of granular material affects the evaluation of planetary impact and cratering formation [12]. In civil and geotechnical engineering, vibrations may affect soil strength and stability [13].

Recently, experimental studies have started to investigate the effect of vibrations in confined granular materials. Xie et al. [14] investigated the effect of vibrations in shear strength in triaxial experiments. A clear strength reduction may be observed depending on factors such as amplitude and frequency of the vibrations. Zhou et al. [15] studied the effect of vibrations in friction of dry sand with steel interfaces, observing a reduction in the friction angle. Taslagyan et al. [16] performed experiments on a direct shear apparatus subjected to horizontal vibration, observing the reduction of the friction angle of the material. While experimental data is essential to understand the

impact of vibration in granular materials, numerical simulations can both assist in understanding the underlying mechanisms of the experimental phenomena, and provide a way to extrapolate observed behaviors to different conditions.

The discrete element method (DEM)[17, 18] allows the numerical simulation of an assembly of granular particles. The response of the granular system is simulated at the scale of the particle, using Newton's law, constitutive relations for the stiffness, friction and damping of the contacts, and geometrical consideration of the grains. DEM has been used to understand emergent properties of granular systems by modeling particle interactions. Lemrich et al. [19] and Reichhardt et al. [20] simulated the elastic modulus softening due to vibrations in confined granular materials using DEM. Zhou et al. [21] studied the effect of cyclic loading in resistance of confined granular materials motivated by the occurrence of slope instability during earthquakes. Ferdowsi et al. [22] simulated confined sheared granular layers applying it to earthquake dynamics. Clark et al. [23] and Zhang et al. [24] studied the effect of vibration in direct shear tests using DEM.

This paper will use DEM to model the effect of vibrations in a granular system subjected to a triaxial confinement. Numerical experiments are performed in order to assess the impact of vibration amplitude and frequency on the angle of internal friction and dilatancy of the material.

## 2 Methodology

### 2.1 Discrete element simulation

The discrete element simulation [17] is described in this section. The simulation is performed using Yade open-source software [25]. Approximately 1200 spherical particles are used. The displacement and velocity of the particles are calculated at each time step as a function of applied forces in each individual particles.

In the current model, the applied forces develop from shear and compression interactions between each particle (Figure 1 a). Spherical particles have individual Young modulus in the normal contact direction  $E_N$ , Young modulus in the tangential direction  $E_T$  (defined as a ratio  $E_T/E_N$ ), density  $\rho$ , normal damping ratio  $\beta_n$  and friction coefficient  $\mu$ . The effective properties of contact forces are calculated based on the individual properties of the particles. The effective stiffness of normal contact  $K_N$  is calculated as an effective stiffness due to two springs in series:

$$K_N = \frac{E_{N1}l_{p1}E_{N2}l_{p2}}{E_{N1}l_{p1} + E_{N2}l_{p2}} \quad (1)$$

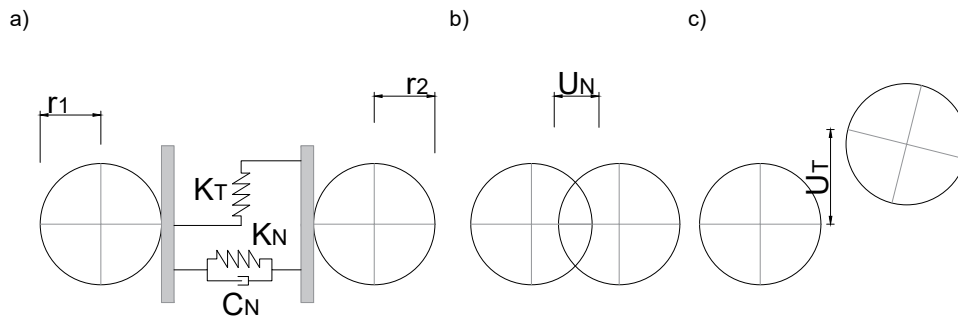


Figure 1. a) Representation of stiffness of the contacts. b) Normal displacements. c) Tangential displacements.

where  $E_{N1}$  and  $E_{N2}$  are the Young modulus of the particles in contact, and  $l_{pi}$  and is a reference length value, considered as the diameter of each particle  $i$ . The effective stiffness  $K_T$  of tangential contact is similarly calculated as springs in series. With the effective stiffness properties of the contacts, the normal and tangential forces ( $F_N$  and  $F_T$ , respectively) may be calculated as:

$$F_N = U_N K_N \quad (2)$$

$$F_T = U_T K_T \quad (3)$$

where  $U_N$  and  $U_T$  are the normal and tangential displacements of the contact (Figure 1b and c).

The effective normal damping coefficient  $C_N$  is calculated as a function of the average normal damping ratio  $\beta_n$  of the particles in contact as  $C_N = \beta_n 2\sqrt{m} * \overline{Kn}$  where  $m$  is the effective mass calculated from  $\rho$  and the geometry.

Numerical time integration is performed using a time step as a fraction of the critical time step. The critical time step is estimated based on the stiffness and density of the particles as

$$\Delta t_{cr} = \min_i r_i \sqrt{\frac{\rho_i}{E_i}} \quad (4)$$

## 2.2 Triaxial cell

The simulated triaxial cell is composed of boundary walls forming a prismatic cell, enclosing the discrete particles. The prism has reference dimensions  $L_x$ ,  $L_y$  and  $L_z$  (Figure 2a). Throughout the analysis, the lateral walls move, changing the prismatic cell dimensions to  $l_x$ ,  $l_y$  and  $l_z$  (Figure 2b). The stresses in the cell are a function of the total forces applied at a wall and its area considering the current dimension (Figure 2c). In this paper, logarithmic strains are used, and the strain can be calculated as  $\varepsilon_i = \ln(l_i/L_i)$ . The volumetric strain is calculated as  $\varepsilon_v = \varepsilon_x + \varepsilon_y + \varepsilon_z$ .

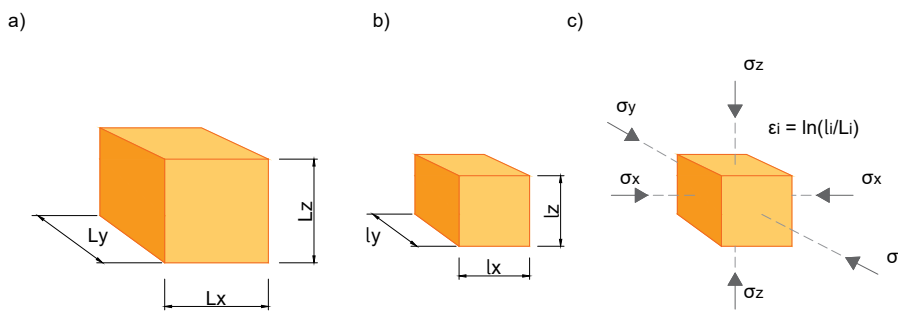


Figure 2. Methodology of the numerical experiments. a) Reference dimensions of the triaxial cell. b) Current dimensions as the triaxial cell moves. c) Stress and strains of the triaxial cell.

The spherical particles and walls had the following properties: Young modulus  $E_N = 1 \cdot 10^8 Pa$ ,  $E_T/E_N = 0.3$ ,  $\beta_n = 0.3$ , density  $\rho = 1000 kg/m^3$ . Particles had friction coefficient  $\mu = 0.3$ , and walls had  $\mu_{wall} = 0$ . The particles had constant radius equal to  $r = 0.01m$ , and are created in a cubic domain with side length  $L = 0.3m$ . The reference length is defined as the length, height and width of the cell when the isotropic compression phase ends, which is generally different from  $L = 0.3$ . It is important to note that real granular materials—such as soil, food grains, glass beads, plastics, and others—exhibit a wide range of physical properties. Therefore, a single set of physical parameters was adopted here, not to represent any specific material, but rather as a generic reference point within the spectrum of possible values and scales of the problem. Future studies should explore the effects of varying these physical parameters to better understand their influence on the system.

## 2.3 Sample preparation and triaxial experiments

The triaxial experiment is composed of three phases. Initially, isotropic compression is performed using Yade's *TriaxialStressController* algorithm [25], which controls the walls' displacement iteratively, in order to confine the granular material to a desired stress level  $\sigma_x = \sigma_y = \sigma_z = P$ , which is equal to  $P = 40kPa$ . In this phase, at each time step the difference between the desired stress and current stress is checked, and the wall's displacement is changed accordingly. After some time steps, the stress stabilizes to a desired approximation of  $P$ . The ratio  $E_N/P = 10^4$  is in the range where the effect of the Young modulus starts to be negligible [26] in this phase. Figure 3 shows the confined particles. In order to create a relatively consolidated sample, in the initial confinement phase, the frictional coefficient  $\mu$  between the spherical particles is set to zero. In the subsequent phases, the friction between particles is activated. When the friction is activated, the friction coefficient  $\mu$  is constant. There is no difference between static and dynamic friction in the current model.

In the second phase, a monotonic strain  $\varepsilon_z = 0.01$  is imposed, while normal stresses  $\sigma_y = \sigma_x = P$  are maintained in the lateral walls. Normal stresses  $\sigma_z$  in the top and bottom boundaries and volumetric strains  $\varepsilon_v$

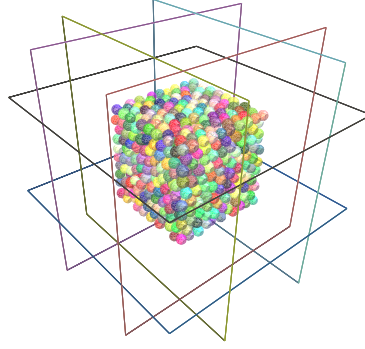


Figure 3. 3D model of the granular material under isotropic compression.

are observed as a function of vertical strain  $\varepsilon_z$ . In this monotonic phase, the Inertial Number is  $I_n = \dot{\varepsilon}_z(r \cdot 2)/(\sqrt{P/\rho}) = 3.16 \cdot 10^{-5}$ , which is low enough to avoid inertial effects [27].

Finally, in the third phase, the monotonic strain is stopped, and vibration is imposed in the top and bottom boundaries, by application of a senoidal strain rate, and the effect of the vibration in the stress and volumetric strain is observed. Changes due to amplitude and frequency of the vibrations are investigated.

Monotonic and vibratory strain can be controlled by imposing a strain rate  $\dot{\varepsilon}_z(t)$  as a function of time  $t$ , and the axial strain is defined as  $\varepsilon_z(t) = \dot{\varepsilon}_z(t)\Delta t$ . When the vibration is imposed, the strain rate is defined as:

$$\dot{\varepsilon}_z(t) = A_v \sin(2\pi f_v t), \quad (5)$$

where  $A_v$  is the amplitude of the vibration strain rate and  $f_v$  is the frequency of the vibration, and  $t$  is the time of the simulation. Then, the strain  $\varepsilon_z$  and strain acceleration  $\ddot{\varepsilon}_z$  are simply:

$$\varepsilon_z(t) = -\frac{A_v}{2\pi f_v} \cos(2\pi f_v t) \quad (6)$$

$$\ddot{\varepsilon}_z(t) = -A_v 2\pi f_v \sin(2\pi f_v t) \quad (7)$$

And finally, the strain amplitude  $A_d$  and acceleration strain amplitude  $A_a$  may be defined as  $A_d = A_v/(2\pi f_v)$  and  $A_a = A_v 2\pi f_v$ . Notice that the acceleration frequency and displacement frequency remains equal to  $f_v$ .

The effect of gravity is neglected in the the analysis, since the pressure effect is considerably greater. The walls' friction coefficient  $\mu_{wall}$  is zero throughout the whole experiment. It is important to note that the effect of the amplitude and frequency is associated with the scale of the material parameters used, and future studies may further investigate how different scales of vibration and physical parameters affect the result. That being said, phenomena of interest may include those with relatively high frequency, such as particles in contact to vibrating machinery or stiff structures. Additionally, the granulometry and shape of the particles are expected to have some influence in both the internal friction angle and the volumetric evolution of the material. In this study, for simplicity, spherical particles of uniform size are employed. For a discussion of the effect of grain shape in a similar context, see Taslagyan et al. [16].

The response of the granular system will be evaluated through its internal friction angle  $\phi$  and its volumetric dilatancy response  $\varepsilon_v$  given as a function of axial strain  $\varepsilon_z$ . The friction angle is calculated as

$$\phi = \sin^{-1} \left( \frac{\sigma_z - P}{\sigma_z + P} \right), \quad (8)$$

The deviatoric stress  $q = \sigma_z - P$  is also used to assess the results when plotting the stress-strain curve. Since  $\sigma_z$  continuously changes throughout the analysis, the change in friction angle due to vibration  $\Delta\phi$  will be evaluated with two stress values at the two significant moments in time: at the end the monotonic compression phase (the second phase) defined as  $\sigma_z^{point A}$  and the average stress in time (calculated with a moving window)  $\bar{\sigma}_z^{point B}$  at the end of the third phase. Using the average value in time during the vibration is useful so that the amplitude of the stress change does not impact the result. The change in friction angle is defined as  $\Delta\phi = \phi^{point A} - \phi^{point B}$ .

### 3 Results

The effect of vibration in the triaxial test for the granular material is presented in this section. Initially, the standard triaxial test is performed without vibration. The stress-strain curve and dilatancy behavior are presented

in Figure 4a and 4b, respectively. Then, the same experiment (including the same configuration of initial particle's positions and properties) is performed with the application of vibration, with strain rate amplitude  $A_v = 0.735$  and frequency  $f_v = 125Hz$ , which leads to strain amplitude  $A_d = 0,93\%$  and strain acceleration amplitude of  $A_a = 577$ . The effect of vibration in the stress-strain curve and dilatancy behavior is presented in Figure 4a and 4b, respectively.

It is noticeable the impact of vibration on the strength reduction and decrease of the volumetric strain of the material. For the imposed vibration, the material exhibits a drop in normal vertical stress  $\sigma_z$  and a decrease in the volumetric strain. The change in strength for this confinement level can also be seen in Figure 5a), where the stress is plotted as a function of time. It can be seen that the effect of vibration is greater at the beginning of the vibration phase, with a smaller effect as time progresses.

The reduction of the friction angle is defined comparing the friction angle on the onset of vibration application (Point A in Figures 4 and 5), calculated as  $\phi^{point A} = 22.24^\circ$  and the friction angle from the average stress during the application of vibration, calculated from a moving window (Point B in Figures 4 and 5),  $\phi^{point B} = 11.15^\circ$ , resulting in a variation of internal friction angle of  $\Delta\phi = -11.09^\circ$ .

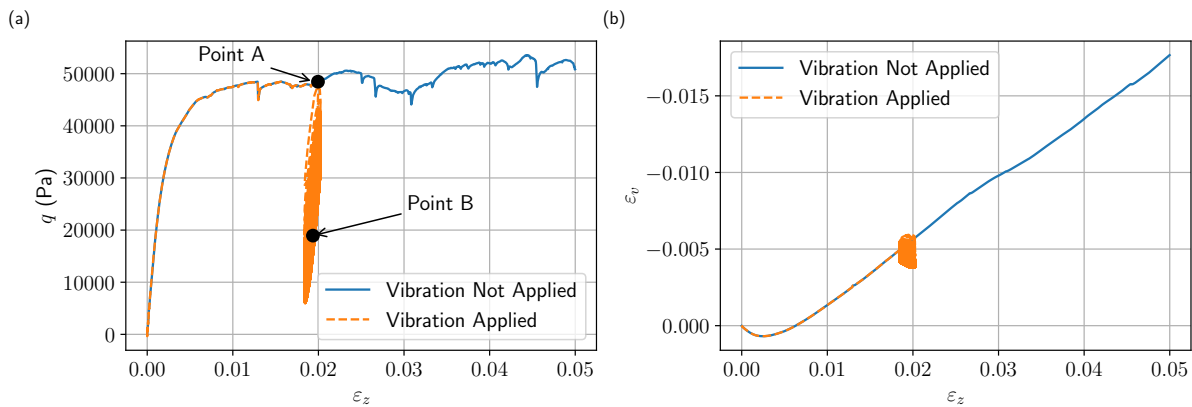


Figure 4. Effect of vibration ( $A_v = 0.735$  and frequency  $f_v = 125Hz$ ) on the triaxial test when vibration is applied at 0.02 strain level. a) Stress-strain curve and strength reduction. b) Dilatancy behavior.

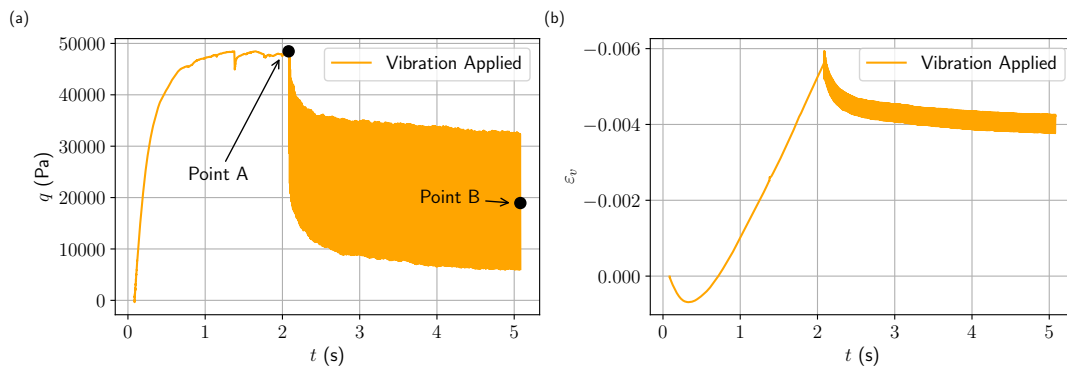


Figure 5. Effect of the number of cycles of vibration ( $A_v = 0.735$  and frequency  $f_v = 125Hz$ ). a) Shear strength reduction as a function of time  $t$ . b) Volumetric strain  $\varepsilon_v$  as a function of time  $t$ .

The effect of the amplitude and frequency of the vibration in the stress-strain curve and dilatancy behavior is further investigated considering the same previous conditions. First, the amplitude of the strain rate is varied from  $A_v = 0.061$  to  $A_v = 1.47$  for constant frequency  $f_v = 125Hz$ . The reduction in the friction angle  $\Delta\phi$  is presented in Figure 6a). As it can be seen the amplitude directly impacts the strength reduction of the material. The volumetric strain was also affected, and the greatest amplitudes had an impact of approximately 70% and the smaller amplitude had an impact of only 0.06% on the volumetric strain.

The impact of the frequency  $f_v$  is also assessed while the strain rate amplitude  $A_v$  changes in the same proportion. This way,  $A_d$  is kept constant and equal to  $A_d = 0,93\%$  and  $A_a$  changes continuously. Figure 6b) presents the change in friction angle  $\Delta\phi$  as a function of  $f_v$ . Further studies may be conducted to check if the

behavior is linear, exponential or follows another pattern. It is observed, however, that the maximum reduction is the static friction angle of  $22.24^\circ$  of the current sample.

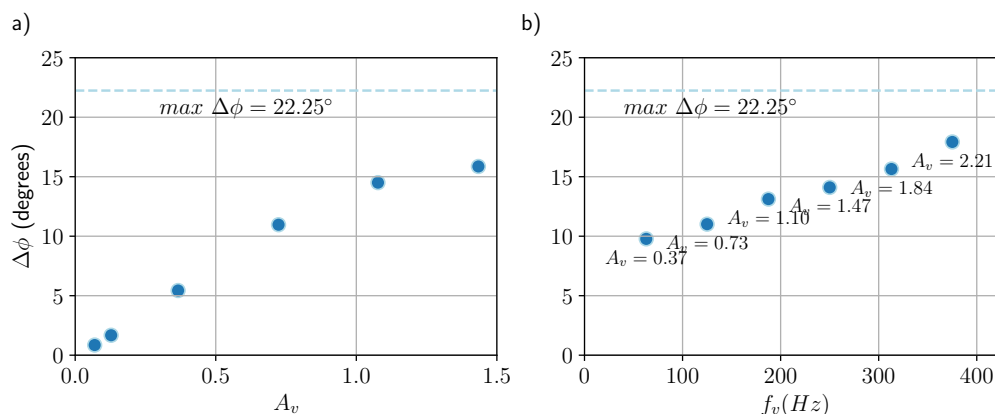


Figure 6. Effect of amplitude  $A_v$  and frequency  $f_v$  of vibration in the friction angle reduction  $\Delta\phi$ . a) Effect of amplitude  $A_v$  of vibration. b) Effect of frequency  $f_v$  of vibration considering the change in  $f_v$  while keeping  $A_d = 0.93\%$  constant.

The present results show that the strength reduction and dilatancy impact can be observed in the current model. The reductions in the friction angle due to vibration has been experimentally observed in the literature [28] and the reduction in volumetric strain has also been reported [14] with sand. It is interesting that in the current simulation, no difference between static and dynamic coefficient of friction was necessary to be considered to observe the effects in the response due to vibration.

## 4 Conclusions

The current paper investigated the effect of vibrations in the strength and dilatancy of confined granular materials using discrete element simulations. The simulation indicates that vibration can cause shear strength reduction and volumetric strain modification in the triaxial experiment. A clear relationship between the amplitude of the strain rate vibration  $A_v$ , the frequency  $f_v$  and the internal friction angle was observed for the current model. The volumetric strain was also impacted by the vibration, and the change in amplitude can have a considerable impact on the material's response. For one specific sinusoidal strain rate, the change in strength and volumetric conditions may change through the time of application, where a sudden drop is first observed, followed by a tendency of stabilization. The discrete element simulation presents similar behaviors to experimental tests. Further studies may investigate the impact of a greater range of amplitude and frequency values, different inertial and stiffness conditions, and also the impact of the friction coefficient and further scaling effects in the model's response.

### Acknowledgements.

We gratefully acknowledge the support of Total Energies Brazil and FUNCAMP (process 4682-23), and the Brazilian National Council for Scientific and Technological Development - CNPq (Process # 308040/2021-0)

### Authorship statement.

The authors hereby confirm that they are the sole liable persons responsible for the authorship of this work, and that all material that has been herein included as part of the present paper is either the property (and authorship) of the authors, or has the permission of the owners to be included here.

## References

- [1] A. Mehta and G. Barker. The dynamics of sand. *Reports on Progress in Physics*, vol. 57, n. 4, pp. 383, 1994.
- [2] A. Kudrolli. Size separation in vibrated granular matter. *Reports on Progress in Physics*, vol. 67, n. 3, pp. 209–247, 2004.
- [3] Q. Guo, C. Spitler, J. M. Sanghishetty, and C. M. Boyce. Advances in vibrated gas-fluidized beds. *Current Opinion in Chemical Engineering*, vol. 42, pp. 100977, 2023.

- [4] N. Denies and A. Holeyman. Shear strength degradation of vibrated dry sand. *Soil Dynamics and Earthquake Engineering*, vol. 95, pp. 106–117, 2017.
- [5] N. Denies, J. Canou, J.-N. Roux, and A. Holeyman. Vibrocompaction properties of dry sand. *Canadian Geotechnical Journal*, vol. 51, n. 4, pp. 409–419, 2014.
- [6] L. Tong, B. Qi, H. Ding, and C. Xu. Statistical model predicts softening and fluidization induced by vibration in granular materials. *International Journal of Mechanical Sciences*, vol. 171, pp. 105373, 2020.
- [7] T. Xie, P. Guo, and D. Stolle. Thermodynamic basis of granular stz model and its application in revealing shear resistance reduction mechanisms of granular soils under vibration. *Continuum Mechanics and Thermodynamics*, vol. 35, n. 6, pp. 2239–2253, 2023a.
- [8] C. K. C. Lieou, A. E. Elbanna, J. S. Langer, and J. M. Carlson. Stick-slip instabilities in sheared granular flow: The role of friction and acoustic vibrations. *Physical Review E*, vol. 92, n. 2, 2015.
- [9] T. Xie, P. Guo, and D. Stolle. Development of extended stz model for granular soils subjected to combined static loading and vibration. *Géotechnique*, vol. 0, n. 0, pp. 1–9, 0.
- [10] C. K. C. Lieou, A. E. Elbanna, and J. M. Carlson. Dynamic friction in sheared fault gouge: Implications of acoustic vibration on triggering and slow slip. *Journal of Geophysical Research: Solid Earth*, vol. 121, n. 3, pp. 1483–1496, 2016.
- [11] C. K. C. Lieou, E. G. Daub, R. A. Guyer, R. E. Ecke, C. Marone, and P. A. Johnson. Simulating stick-slip failure in a sheared granular layer using a physics-based constitutive model. *Journal of Geophysical Research: Solid Earth*, vol. 122, n. 1, pp. 295–307, 2017.
- [12] H. Katsuragi and others. *Physics of soft impact and cratering*. Springer, 2016.
- [13] T. Wu, C. Zhou, N. Jiang, Y. Xia, and Y. Zhang. Stability analysis for high-steep slope subjected to repeated blasting vibration. *Arabian Journal of Geosciences*, vol. 13, pp. 1–12, 2020.
- [14] T. Xie, P. Guo, and D. Stolle. Experimental and modelling investigation of vibration-induced fluidization in sheared granular soils. *International Journal for Numerical and Analytical Methods in Geomechanics*, vol. 47, n. 8, pp. 1399–1415, 2023b.
- [15] S. Zhou, H. Jiang, L. Fu, Y. Shan, W. Ye, and P. Guo. Experimental study on deformation and strength characteristics of granular soil-structure interface under coupled monotonic shear and vibration using a modified direct shear apparatus. *Acta Geotechnica*, vol. 18, n. 6, pp. 2899–2913, 2022.
- [16] K. A. Taslagyan, D. H. Chan, and N. R. Morgenstern. Vibrational fluidization of granular media. *International Journal of Geomechanics*, vol. 16, n. 3, pp. 04015080, 2016.
- [17] P. A. Cundall and O. D. Strack. A discrete numerical model for granular assemblies. *geotechnique*, vol. 29, n. 1, pp. 47–65, 1979.
- [18] C. Thornton. *Granular dynamics, contact mechanics and particle system simulations*, volume 24. Springer, 2015.
- [19] L. Lemrich, J. Carmeliet, P. A. Johnson, R. Guyer, and X. Jia. Dynamic induced softening in frictional granular materials investigated by discrete-element-method simulation. *Physical Review E*, vol. 96, n. 6, 2017.
- [20] C. J. O. Reichhardt, L. M. Lopatina, X. Jia, and P. A. Johnson. Softening of stressed granular packings with resonant sound waves. *Physical Review E*, vol. 92, n. 2, 2015.
- [21] X.-H. Zhou, Y.-G. Zhou, and Y.-M. Chen. Dem analysis of undrained cyclic behavior and resistance of saturated dense sand without stress reversals. *Granular Matter*, vol. 25, n. 2, 2023.
- [22] B. Ferdowsi, M. Griffa, R. A. Guyer, P. A. Johnson, and J. Carmeliet. Effect of boundary vibration on the frictional behavior of a dense sheared granular layer. *Acta Mechanica*, vol. 225, n. 8, pp. 2227–2237, 2014.
- [23] A. H. Clark, E. E. Brodsky, H. J. Nasrin, and S. E. Taylor. Frictional weakening of vibrated granular flows. *Physical Review Letters*, vol. 130, n. 11, 2023.
- [24] Z. Zhang, Y. Cui, D. H. Chan, and K. A. Taslagyan. Dem simulation of shear vibrational fluidization of granular material. *Granular Matter*, vol. 20, n. 4, 2018.
- [25] V. Smilauer, V. Angelidakis, E. Catalano, R. Caulk, B. Chareyre, W. Chevremont, S. Dorofeenko, J. Duriez, N. Dyck, J. Elias, and others. *Yade documentation*, 2023.
- [26] F. Da Cruz, S. Emam, M. Prochnow, J.-N. Roux, and F. Chevoir. Rheophysics of dense granular materials: Discrete simulation of plane shear flows. *Physical Review E—Statistical, Nonlinear, and Soft Matter Physics*, vol. 72, n. 2, pp. 021309, 2005.
- [27] G. Koval, J.-N. Roux, A. Corfdir, and F. Chevoir. Annular shear of cohesionless granular materials: From the inertial to quasistatic regime. *Physical Review E—Statistical, Nonlinear, and Soft Matter Physics*, vol. 79, n. 2, pp. 021306, 2009.
- [28] W. Ye, L. Fu, Y. Shan, N. Dai, P. Guo, S. Zhou, and F. Rackwitz. Experimental study on dynamic characteristics of granular materials under axial high-frequency vibration. *Acta Geotechnica*, vol. 17, n. 8, pp. 3211–3227, 2022.